CEA Comité Español de Automática
XLVI JORNADAS AUTOMÁTICA CARTAGENA 2025
UNIVERSIDADE DA CORUÑA

Jornadas de Automática

Fault diagnosis using residuals generation for anion exchange membrane water electrolyzer

Assia, Hamza*, Meftah, Imad Zakaria, Camacho, Pablo G., Belkedari, Meriem, Rouzbehi, Kumars, Escaño, Juan Manuel

Departamento de Ingeniería de Sistemas y Automática, Universidad de Sevilla, C/ Camino de los Descubrimientos, s/n, 41092, Sevilla, España.

To cite this article: Hamza, Assia, Imad Zakaria, Meftah, Camacho, Pablo G., Meriem, Belkedari, Kumars, Rouzbehi, Escaño, Juan M. 2025. Fault diagnosis using residual generation for AEM water electrolyzer. Jornadas de Automática, 46. https://doi.org/10.17979/ja-cea.2025.46.12267

Resumen

Los electrolizadores de membrana de intercambio aniónico (AEMWE) representan una tecnología prometedora para la producción de hidrógeno limpio, aunque son susceptibles a fallos que pueden afectar su rendimiento y seguridad. Este artículo presenta un marco de diagnóstico de fallos basado en modelos para AEMWE, utilizando observadores no lineales y generación de residuos. Se desarrolla un modelo no lineal en espacio de estados que captura las principales dinámicas electroquímicas y de transporte del sistema. A partir de este modelo, se diseña un observador no lineal tipo Luenberger para la estimación de estados internos, y se propone una estrategia estructurada de generación de residuos para la detección y aislamiento de fallos específicos. La metodología se evalúa ante tres escenarios de fallo: un fallo en el actuador de corriente, un sesgo en el sensor de voltaje y un desplazamiento en el sensor de caudal de hidrógeno. Cada fallo se identifica mediante firmas residuales distintas, lo que permite un diagnóstico fiable. Los resultados de simulación validan la eficacia del enfoque propuesto, demostrando su potencial para mejorar la fiabilidad y seguridad operativa de los sistemas AEMWE.

Palabras clave: AEM Water Electrolyzer, Fault Diagnosis, State-Space Modeling, Nonlinear Observers, Residual Generation.

Fault Diagnosis using Residuals Generation for AEM Water Electrolyzer

Abstract

Anion Exchange Membrane Water Electrolyzers (AEMWEs) are a promising technology for clean hydrogen production, yet they remain vulnerable to faults that can impair performance and safety. This paper presents a model-based fault diagnosis framework for AEMWEs using nonlinear observers and residual generation. A comprehensive nonlinear state-space model is developed to capture the key electrochemical and transport dynamics of the system. A Luenberger-type nonlinear observer is designed to estimate the internal states, and a structured residual generation strategy is proposed to detect and isolate specific faults. The method is evaluated under three fault scenarios: a current actuator fault, a voltage sensor bias, and a hydrogen flow sensor offset. Each fault is identified through distinct residual signatures, enabling reliable diagnosis. Simulation results validate the effectiveness of the proposed scheme, demonstrating its potential to enhance the operational reliability and safety of AEMWE systems.

Keywords: AEM Water Electrolyzer, Fault Diagnosis, State-Space Modeling, Nonlinear Observers, Residual Generation.

1. Introduction

Hydrogen is rapidly gaining prominence as a clean energy carrier, providing a sustainable alternative to fossil fuels in various sectors, including energy storage, industrial processes, and transportation (Muradov and Veziroğlu, 2008). Among hydrogen production technologies, water electrolysis is particularly attractive due to its ability to produce high purity hydrogen directly from water, especially when powered by rene-

*Autor para correspondencia: hassia@us.es
Attribution-NonCommercial-ShareAlike 4.0 International (CC BY-NC-SA 4.0)

wable electricity (Shiva Kumar and Himabindu, 2019). Anion Exchange Membrane (AEM) water electrolyzers are attracting significant attention due to their potential to combine the advantages of Proton Exchange Membrane (PEM) and alkaline electrolyzers, such as high efficiency, dynamic operation, and the use of non-precious metal catalysts (Qayoom et al., 2024).

However, like other electrochemical systems, AEM water electrolyzers are susceptible to various faults that may degrade performance, reduce lifespan, or lead to unsafe operating conditions. Common faults include membrane wear, catalyst degradation, sensor errors, actuator malfunctions, and disruptions in process control (Ding, 2013). Therefore, effective fault diagnosis is critical for ensuring safe, reliable, and efficient operation, minimizing downtime, and optimizing maintenance strategies. Model-based fault diagnosis techniques, which compare system behavior to a mathematical model by generating residuals, have proven to be robust and effective in various industrial applications (Ding, 2013).

Despite significant research in the modeling and control of AEM electrolyzers, systematic application of classical model-based fault diagnosis methods, particularly those employing nonlinear observers and residual generation, remains an area requiring further exploration. This paper addresses this gap by developing a detailed state-space model of an AEM electrolyzer and proposing a classical fault diagnosis framework.

This work presents several key contributions aimed at enhancing fault diagnosis in AEM water electrolyzers. First, a detailed nonlinear state-space model is developed to accurately represent the fundamental electrochemical and transport dynamics of the system. Building on this model, a nonlinear observer is designed to estimate internal states, providing the foundation for detecting deviations in system behavior. A residual generation strategy is then formulated, specifically tailored to identify faults such as deviations in current actuation or voltage sensing. Finally, a fault signature table and detection logic are established, enabling clear identification and differentiation of fault types based on residual patterns.

The remainder of this paper is organized as follows: Section 2 presents the mathematical state-space model of the AEM electrolyzer. Section 3 introduces the fault modeling. Section 4 describes the observer-based fault diagnosis framework, including the nonlinear observer design, residual generation, error dynamics, and fault detection logic. Section 5 presents the simulation results. Finally, Section 6 concludes the paper and outlines directions for future work.

2. Mathematical State-Space Model for AEM Water Electrolyzer

The electrochemical and transport phenomena of the AEM Water Electrolyzer are modeled using the following equations. This section details the complete state-space representation of the system.

2.1. Model Description

The cell voltage E_{cell} in [V] is defined as (Gomez Vidales et al., 2023),

$$E_{cell} = E_{rev} + \eta_{act} + \eta_{ohm} + \eta_{diff} \tag{1}$$

where,
E_{rev} is the required voltage for the electrolysis reaction [V].
η_{act} is the activation overpotential [V].
η_{ohm} is the voltage loss [V].
η_{diff} is effect of mass transport processes and the concentration effects, in particular diffusion processes.

The activation Overpotential (Butler-Volmer) is given by (Dickinson and Wain, 2020),

$$\eta_{act} = \frac{RT}{anF} \ln\left(\frac{i}{i_0}\right) \tag{2}$$

The ohmic resistances arise from the electrical resistances within the electrolyzer cell and can be described using Ohm's law (Phillips et al., 2017),

$$\eta_{ohm} = i \cdot (r_{KOH} + r_{mem}) \tag{3}$$

The activation overpotential η_{act} represents the energy needed to overcome the activation barriers of the HER and OER, as determined by reaction kinetics (Roy et al., 2006),

$$\eta_{diff} = \frac{RT}{4F} \ln\left(\frac{C_{O_2,mem} \cdot C_{H_2,mem}}{C_{O_2,mem,0} \cdot C_{H_2,mem,0}}\right) \tag{4}$$

where,
R is universal gas constant 8.3145 $[Jmol^{-1}K^{-1}]$.
T is the absolute temperature $[K]$.
F is Faraday constant 96485 $[Cmol^{-1}]$.
$C_{O_{mem},2}$ is the oxygen and hydrogen concentration at the membrane/electrolyte interface $[molm^{-3}]$.
$C_{H_{mem},2}$ is the hydrogen concentration at the membrane/electrolyte interface $[mol^{-3}]$.
$C_{O_{0mem},2}$ is the oxygen and hydrogen concentration at the membrane/electrolyte interface at working condition taken as a reference $[mol^{-3}]$.
$C_{H_{0mem},2}$ is the hydrogen concentration at the membrane/-electrolyte interface working condition taken as a reference $[mol^{-3}]$.
Hydrogen Production Rate (Faraday's Law) is the molar fluxes (n) of H through the porous electrode can be calculated via Faraday's Law, where the gas production rate at each electrode is normalized by the membrane area (Rizwan et al., 2021),

$$\dot{n}_{H_2} = \frac{i}{2FA} \tag{5}$$

where,
A is the contact area of membrane–electrode assembly $[m^2]$.

2.2. General Non-Linear State-Space Form

The general non-linear state-space form of a dynamic system is given by:

$$\dot{x}(t) = f(x(t), u(t)) \tag{6}$$

$$y(t) = h(x(t), u(t)) \tag{7}$$

where,
$x(t)$ is the vector of state variables.
$u(t)$ is the vector of inputs.
$y(t)$ is the vector of outputs.
f, h is the non-linear vector functions.

2.3. State, Input, and Output Definitions

From the physical modeling of the AEMWE, we define:

State Variables $x(t)$ The chosen state variables vector is given by,

$$x(t) = \begin{bmatrix} C_{H_2,mem} \\ C_{O_2,mem} \\ \lambda \\ T \\ P \end{bmatrix} \tag{8}$$

where,
$C_{H_2,mem}$ is the hydrogen concentration at membrane.
$C_{O_2,mem}$ is the oxygen concentration at membrane.
λ is the state variable lambda. T is the temperature.
P is the operating pressure.

Input Variables $u(t)$ The selected input variables vector is given by,

$$u(t) = \begin{bmatrix} i \\ m \end{bmatrix} \tag{9}$$

where,
i is the applied current.
m is the electrolyte molarity.

Output Variables $y(t)$ The output variables vector is given by,

$$y(t) = \begin{bmatrix} E_{cell} \\ \eta \\ \dot{n}_{H_2} \end{bmatrix} \tag{10}$$

where,
E_{cell} is the cell voltage.
η is the voltage efficiency.
$\dot{n}_{H_2}$ is the hydrogen molar production rate.

2.4. Matrix A(x, u) — State-to-State Dynamics

The state-to-state dynamics of the system is given by,

$$A(x,u) = \begin{bmatrix} -\frac{1}{\tau_{H_2}} & 0 & 0 & \frac{\partial C_{H_2}}{\partial T} & \frac{\partial C_{H_2}}{\partial P} \\ 0 & -\frac{1}{\tau_{O_2}} & 0 & \frac{\partial C_{O_2}}{\partial T} & \frac{\partial C_{O_2}}{\partial P} \\ 0 & 0 & -\frac{1}{\tau_\lambda} & \frac{\partial \lambda}{\partial T} & \frac{\partial \lambda}{\partial P} \\ 0 & 0 & 0 & 0 & 0 \\ 0 & 0 & 0 & 0 & 0 \end{bmatrix} \tag{11}$$

2.5. Matrix B(x, u) — Input-to-State Influence

The input-to-state Influence matrix is given by,

$$B(x,u) = \begin{bmatrix} \frac{\partial C_{H_2}}{\partial i} & \frac{\partial C_{H_2}}{\partial m} \\ \frac{\partial C_{O_2}}{\partial i} & \frac{\partial C_{O_2}}{\partial m} \\ \frac{\partial \lambda}{\partial i} & \frac{\partial \lambda}{\partial m} \\ \frac{\partial T}{\partial i} & \frac{\partial T}{\partial m} \\ \frac{\partial P}{\partial i} & \frac{\partial P}{\partial m} \end{bmatrix} \tag{12}$$

2.6. Matrix C(x, u) — State-to-Output Mapping

The state-to-output is interpreted by,

$$C(x,u) = \begin{bmatrix} \frac{\partial E_{cell}}{\partial C_{H_2}} & \frac{\partial E_{cell}}{\partial C_{O_2}} & \frac{\partial E_{cell}}{\partial \lambda} & \frac{\partial E_{cell}}{\partial T} & \frac{\partial E_{cell}}{\partial P} \\ \frac{\partial \eta}{\partial C_{H_2}} & \frac{\partial \eta}{\partial C_{O_2}} & \frac{\partial \eta}{\partial \lambda} & \frac{\partial \eta}{\partial T} & \frac{\partial \eta}{\partial P} \\ \frac{\partial \dot{n}_{H_2}}{\partial C_{H_2}} & 0 & 0 & 0 & 0 \end{bmatrix} \tag{13}$$

2.7. Matrix D(x, u) — Input-to-Output Coupling

The input-to-output coupling matrix is expressed by,

$$D(x,u) = \begin{bmatrix} \frac{\partial E_{cell}}{\partial i} & \frac{\partial E_{cell}}{\partial m} \\ \frac{\partial \eta}{\partial i} & \frac{\partial \eta}{\partial m} \\ \frac{1}{2F} & 0 \end{bmatrix} \tag{14}$$

3. System Model with Faults

The introduced fault types serve to emulate realistic operational anomalies in AEMWE systems. The current actuator fault $f_i(t)$ represents a deviation in the applied current due to actuator degradation or control error, directly affecting the system's electrochemical dynamics. The voltage sensor fault $f_v(t)$ models a bias or drift in the voltage measurement, which may result from aging sensors or calibration errors and can lead to incorrect control decisions. Finally, the hydrogen flow sensor fault $f_{H_2}(t)$ simulates an offset in the measured hydrogen production rate, typically caused by sensor fouling or drift. These faults are intentionally introduced to evaluate the sensitivity and robustness of the observer-based residual generation framework in detecting and isolating discrepancies between measured and estimated outputs.
The fault-free nonlinear system is described as:

$$\dot{x}(t) = f(x(t), u(t)) \tag{15}$$

$$y(t) = h(x(t), u(t)) \tag{16}$$

where,
$u(t) = \begin{bmatrix} i(t) \\ m(t) \end{bmatrix}$ is the input vector.
$i(t)$ is the current.
$m(t)$ is the water mass flow.
$x(t)$ is the state vector.
$y(t) = \begin{bmatrix} E_{cell}(t) \\ \eta(t) \\ \dot{n}_{H_2}(t) \end{bmatrix}$ is the output vector.

We introduce faults,

- Actuator fault in current: $f_i(t)$
- Voltage sensor fault: $f_v(t)$
- Hydrogen flow sensor fault: $f_{H_2}(t)$

The faulty system becomes,

$$\dot{x}_f(t) = f\left(x_f(t), \begin{bmatrix} i(t) + f_i(t) \\ m(t) \end{bmatrix}\right) \tag{17}$$

$$y_f(t) = \begin{bmatrix} E_{cell}(t) + f_v(t) \\ \eta(t) \\ \dot{n}_{H_2}(t) + f_{H_2}(t) \end{bmatrix} \tag{18}$$

4. Observer-Based Fault Diagnosis

4.1. Nonlinear Observer Design

The observer used is Luenberger and is given by,

$$\dot{\hat{x}}(t) = f\left(\hat{x}(t), \begin{bmatrix} i(t) \\ m(t) \end{bmatrix}\right) + L(y_f(t) - \hat{y}(t)) \tag{19}$$

$$\hat{y}(t) = h\left(\hat{x}(t), \begin{bmatrix} i(t) \\ m(t) \end{bmatrix}\right) \tag{20}$$

4.2. Residual Generation

The residuals are defined as,

$$r(t) = y_f(t) - \hat{y}(t) \tag{21}$$

$$r(t) = \begin{bmatrix} E_{cell}(t) - \hat{E}_{cell}(t) + f_v(t) \\ \eta(t) - \hat{\eta}(t) \\ \dot{n}_{H_2}(t) - \hat{\dot{n}}_{H_2}(t) + f_{H_2}(t) \end{bmatrix} \tag{22}$$

4.3. Estimation Error Dynamics

We define the estimation error,

$$e(t) = x(t) - \hat{x}(t) \tag{23}$$

Linearizing around an operating point,

$$\delta\dot{x}(t) = A\delta x(t) + B\delta u(t) + B_f \begin{bmatrix} f_i(t) \\ 0 \end{bmatrix} \tag{24}$$

$$\delta\dot{\hat{x}}(t) = A\delta\hat{x}(t) + B\delta u(t) + L(\delta y_f(t) - C\delta\hat{x}(t)) \tag{25}$$

Subtracting yields the error dynamics:

$$\dot{e}(t) = (A - LC)e(t) + B_f \begin{bmatrix} f_i(t) \\ 0 \end{bmatrix} - LD_f \begin{bmatrix} f_v(t) \\ 0 \\ f_{H_2}(t) \end{bmatrix} \tag{26}$$

4.4. Linearized Residual Expression

The linearized residual expression is given by,

$$r(t) = Ce(t) + D_f \begin{bmatrix} f_v(t) \\ 0 \\ f_{H_2}(t) \end{bmatrix} \tag{27}$$

4.5. Fault Signature and Detection Logic

We define thresholdsas,

- $|r_{E_{cell}}(t)| > \delta_v \implies$ Voltage fault
- $|r_\eta(t)| > \delta_\eta \implies$ Model mismatch or general fault
- $|r_{\dot{n}_{H_2}}(t)| > \delta_{H_2} \implies$ Hydrogen flow sensor fault

The thresholds for voltage residuals ($\delta_v = 0{,}05\,\text{V}$), hydrogen flow residuals ($\delta_{H_2} = 1 \times 10^{-6}$ mol/s), and efficiency residuals ($\delta_\eta = 0{,}02$) were selected through empirical tuning based on simulations under fault-free conditions. They were set slightly above the maximum residuals observed during normal operation to prevent false alarms. Sensitivity tests confirmed that faults such as a $+0{,}2\,\text{V}$ voltage bias and a $+5\,\mu$mol/s hydrogen flow offset exceeded these thresholds. This demonstrates that the chosen thresholds ensure effective fault detection while maintaining a low false alarm rate.

5. Simulation Results

The simulation results presented in Figure 1 illustrate the behavior of the Anion Exchange Membrane Water Electrolyzer (AEMWE) under three fault scenarios—namely, a current actuator fault, a voltage sensor bias, and a hydrogen flow sensor fault—using the model parameters summarized in Table 2. The actuator fault, applied between $t = 50s$ and $t = 70s$ as a $+10$ A offset in the input current, results in a transient increase in the actual applied current. This leads to a temporary shift in the system's electrochemical dynamics and a corresponding change in the voltage residual. However, the induced deviation does not exceed the detection threshold ($\delta_V = 0{,}05V$), indicating that the observer is sensitive to the disturbance but the fault magnitude remains within tolerable bounds. At $t = 100s$, a voltage sensor fault is introduced by applying a $+0{,}2V$ bias to the measured cell voltage. This creates a noticeable discrepancy between the true and observed voltage values, with the voltage residual exceeding the detection threshold δ_V, thereby allowing the fault to be successfully identified. Subsequently, at $t = 150s$, a hydrogen sensor fault modeled as a $+5\mu mol/s$ offset leads to a sharp increase in the measured hydrogen production rate. This anomaly is promptly detected as the hydrogen residual surpasses the threshold $\delta_{H2} = 1\mu mol/s$. Throughout the simulation, the efficiency residual remains within the detection threshold $\delta_\eta = 0{,}02$, confirming that the voltage efficiency remains unaffected by the injected faults. The initial transient response shows a rapid decay in hydrogen and oxygen concentrations at the membrane interface, stabilizing near zero, while the membrane hydration level (λ), temperature ($T = 333{,}15K$), and pressure ($P = 1atm$) remain constant—indicating the absence of thermal or pressure-related disturbances. Overall, these results confirm the effectiveness of the observer-based residual generation framework for accurately detecting and isolating faults in AEMWE systems. The distinct residual patterns associated with each fault type highlight the capability of the diagnostic scheme to operate reliably under realistic fault conditions.

Table 2: AEMWE Model Parameters Used in Simulation (Gomez Vidales et al., 2023).

Parameter	Value
Universal gas constant (R)	8.314 J/(mol·K)
Faraday's constant (F)	96485 mol
Charge transfer coefficient (α)	0.5
Number of electrons transferred (n)	2
Initial temperature (T_0)	298 K
Initial pressure (P_0)	101325 Pa
Initial membrane concentrations ($C_{H_2,\text{mem},0}$, $C_{O_2,\text{mem},0}$)	0.1 mol/m^3
Initial membrane water content (λ_0)	10
H_2 transport time constant (τ_{H_2})	10.0 s
O_2 transport time constant (τ_{O_2})	10.0 s
Membrane hydration time constant (τ_λ)	5.0 s
Electrolyte resistance (KOH) (r_{KOH})	0.1 Ω·m^2
Membrane resistance (r_{mem})	0.2 Ω·m^2
Exchange current density (i_0)	0.1 A/m^2
Reversible cell voltage (E_{rev})	1.23 V
Voltage residual threshold (δ_V)	0.05 V
Efficiency residual threshold (δ_η)	0.02
Hydrogen residual threshold (δ_{H_2})	1×10^{-6} mol/s

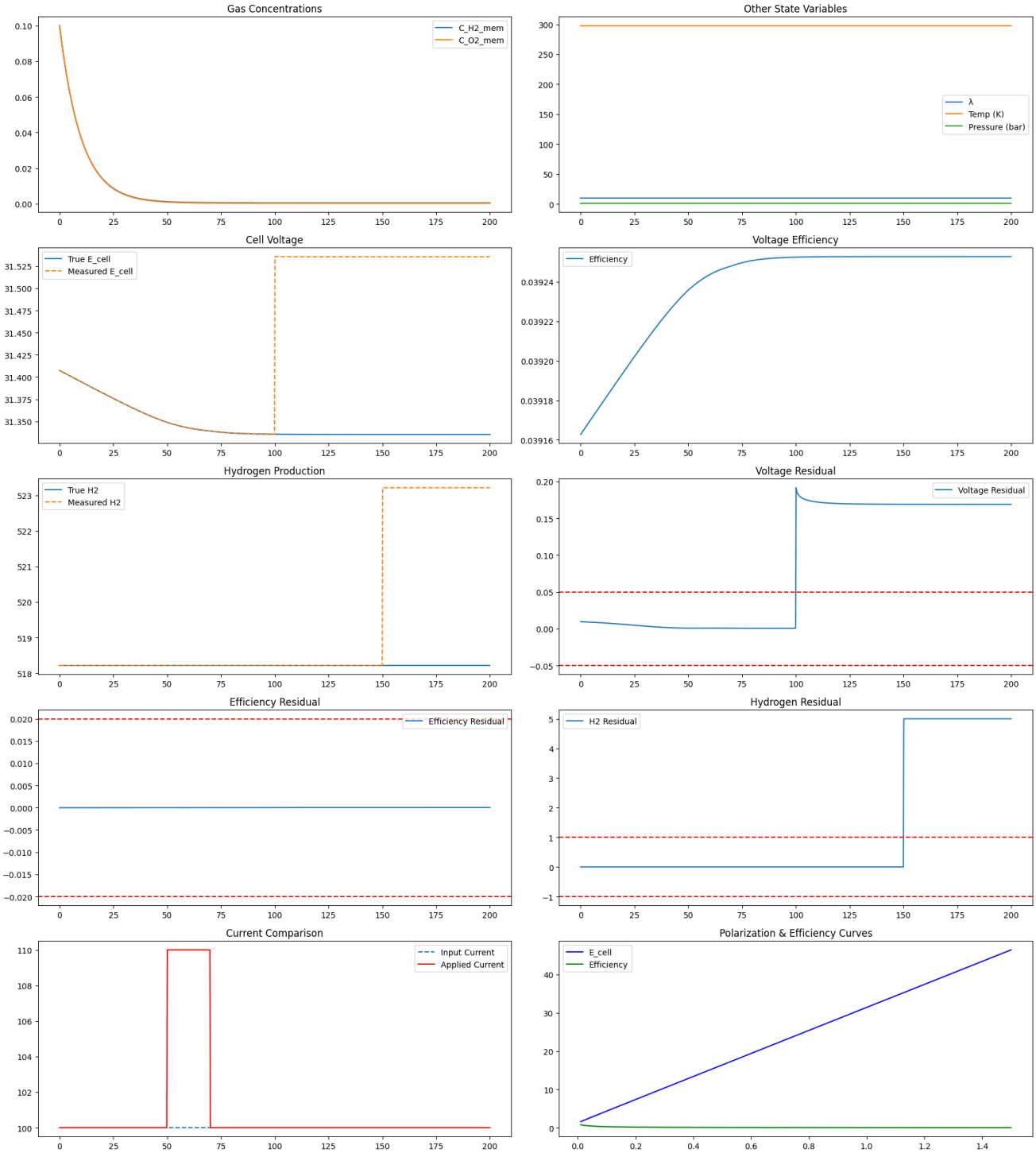

Figure 1: Simulation Result for a Healthy AEMWE.

Table 1: Fault Signature Table

Fault Type	Variable	Affected Residual(s)	Signature
Actuator fault	$f_i(t)$	$r_{E_{cell}}(t)$, $r_{\dot{n}_{H_2}}(t)$	$r_{E_{cell}}(t)$ non-zero, $r_\eta(t)$ near zero
Voltage sensor fault	$f_v(t)$	$r_{E_{cell}}(t)$	$r_{E_{cell}}(t)$ non-zero, $r_\eta(t)$ near zero
Hydrogen flow sensor fault	$f_{H_2}(t)$	$r_{\dot{n}_{H_2}}(t)$	$r_{\dot{n}_{H_2}}(t)$ non-zero, others near zero
No fault	0	All residuals converge to 0	All residuals near zero

6. Conclusion

This paper presents a comprehensive framework for model-based fault diagnosis in Anion Exchange Membrane Water Electrolyzers (AEMWEs) using residual generation. A detailed nonlinear state-space model was developed to capture the system's electrochemical and transport dynamics. Based on this model, a nonlinear observer was designed to estimate the internal states, enabling the generation of residuals. These residuals, sensitive to specific fault types, were used to construct a fault signature table and a detection logic capable of isolating actuator and sensor faults.

The proposed approach demonstrates the feasibility and potential of classical observer-based techniques for enhancing the operational safety of AEMWEs. Early fault detection and isolation contribute to reducing downtime, preventing failures, and optimizing maintenance schedules.

As future work, experimental validation on a real AEM water electrolyzer will be conducted to assess the method's performance under real operating conditions. In addition, a systematic threshold optimization based on statistical analysis will be explored to improve detection accuracy and robustness under varying operational scenarios.

Acknowledgements

The authors acknowledge the financial support from Junta de Andalucía (Consejería de Transformación Económica, Industria, Conocimiento y Universidades) through the research grant *Laboratorio de Ingeniería para la Sostenibilidad Energética y Medioambiental, ENGREEN* (reference QUAL21 006 USE). This work has also received funding from PID2022-142069OB-I00 / AEI / 10.13039/501100011033 / FEDER, EU. Kumars Rouzbehi acknowledges support from a Ramón y Cajal grant (RYC2021-032604-I), funded by MCIN / AEI / 10.13039/501100011033 and the European Union NextGenerationEU / PRTR.

References

Dickinson, E. J., Wain, A. J., 2020. The butler-volmer equation in electrochemical theory: Origins, value, and practical application. Journal of Electroanalytical Chemistry 872, 114145, dr. Richard Compton 65th birthday Special issue.
URL: https://www.sciencedirect.com/science/article/pii/S1572665720303283
DOI: https://doi.org/10.1016/j.jelechem.2020.114145

Ding, S. X., 2013. Model-based fault diagnosis techniques. Springer book.
URL: https://link.springer.com/book/10.1007/978-1-4471-4799-2
DOI: 10.1007/978-1-4471-4799-2

Gomez Vidales, A., Millan, N. C., Bock, C., 2023. Modeling of anion exchange membrane water electrolyzers: The influence of operating parameters. Chemical Engineering Research and Design 194, 636–648.
URL: https://www.sciencedirect.com/science/article/pii/S0263876223002940
DOI: https://doi.org/10.1016/j.cherd.2023.05.004

Muradov, N. Z., Veziroğlu, T. N., 2008. "green" path from fossil-based to hydrogen economy: An overview of carbon-neutral technologies. International Journal of Hydrogen Energy 33 (23), 6804–6839.
URL: https://www.sciencedirect.com/science/article/pii/S036031990801118X
DOI: https://doi.org/10.1016/j.ijhydene.2008.08.054

Phillips, R., Edwards, A., Rome, B., Jones, D. R., Dunnill, C. W., 2017. Minimising the ohmic resistance of an alkaline electrolysis cell through effective cell design. International Journal of Hydrogen Energy 42 (38), 23986–23994.
URL: https://www.sciencedirect.com/science/article/pii/S0360319917330203
DOI: https://doi.org/10.1016/j.ijhydene.2017.07.184

Qayoom, A., Ahmad, M., Hussain, F., Qazi, A., Selvaraj, J., Zainul, R., Krismadinata, Abd Rahim, N., Atamurotov, F., Tran, T., Souayeh, B., Benti, N. E., 11 2024. Recent advances in anion exchange membrane technology for water electrolysis: a review of progress and challenges. Energy Science /& Engineering 12, 5328–5352.
DOI: 10.1002/ese3.1938

Rizwan, M., Alstad, V., Jäschke, J., 2021. Design considerations for industrial water electrolyzer plants. International Journal of Hydrogen Energy 46 (75), 37120–37136, international Symposium on Sustainable Hydrogen 2019.
URL: https://www.sciencedirect.com/science/article/pii/S0360319921034984
DOI: https://doi.org/10.1016/j.ijhydene.2021.09.018

Roy, A., Watson, S., Infield, D., 11 2006. Comparison of electrical energy efficiency of atmospheric and high-pressure electrolysers. International Journal of Hydrogen Energy 31, 1964–1979.
DOI: 10.1016/j.ijhydene.2006.01.018

Shiva Kumar, S., Himabindu, V., 2019. Hydrogen production by pem water electrolysis – a review. Materials Science for Energy Technologies 2 (3), 442–454.
URL: https://www.sciencedirect.com/science/article/pii/S2589299119300035
DOI: https://doi.org/10.1016/j.mset.2019.03.002